WIND ENERGY
Wind Energ. 2003; **6**:179–195 (DOI: 10.1002/we.79)

Improved Modal Dynamics of Wind Turbines to Avoid Stall-induced Vibrations

M. H. Hansen* Wind Energy Department, Risø National Laboratory, PO Box 49, DK-4000 Roskilde, Denmark

Key words:
horizontal axis turbines;
mechanical vibrations;
modal analysis;
optimization

Stall-induced edgewise blade vibrations have occasionally been observed on three-bladed wind turbines over the last decade. Experiments and numerical simulations have shown that these blade vibrations are related to certain vibration modes of the turbines. A recent experiment with a 600 kW turbine has shown that a backward whirling mode associated with edgewise blade vibrations is less aerodynamically damped than the corresponding forward whirling mode. In this article the mode shapes of the particular turbine are analysed, based on a simplified turbine model described in a multi-blade formulation. It is shown that the vibrations of the blades for the backward and forward edgewise whirling modes are different, which can explain the measured difference in aerodynamic damping. The modal dynamics of the entire turbine is important for stability assessments; blade-only analysis can be misleading. In some cases the modal dynamics may even be improved to avoid stall-induced vibrations. Copyright © 2003 John Wiley & Sons, Ltd.

Introduction

A theoretical modal analysis of a three-bladed wind turbine is presented, with the aim of explaining observed differences in aerodynamic damping of two apparently similar modes.[1] Similar results have previously been published,[2] but without the present details on the method and analysis.

Stall-induced vibrations of wind turbine blades have become an issue in the optimized design of stall-regulated wind turbines with increasing rotor diameters. Until the 1990s, no problems with such vibrations had been observed, although work performed in the 1980s indicated that these problems could arise.[3] When one of the first examples of stall-induced vibrations was reported on a 500 kW wind turbine,[4] it led to further investigations which have provided a detailed understanding of the problem.[1,5–8]

From the studies of stall-induced vibrations, different types of solutions have been developed. The common solution for a wind turbine in operation is to change the *stall characteristics* of the blade by placing stall strips on the leading edge of the blade.[8,9] When designing a new blade, this aerodynamic issue must of course be considered in the choice of aerofoil profiles. However, the structural dynamics of the blade is also important for the risk of stall-induced vibrations. The aerodynamic damping of a blade section operating in stall is highly dependent on the *direction of blade vibration* (relative to the rotor plane) associated with the primary bending modes.[5,7,8] For most aerofoil profiles at high angles of attack it can be shown, using quasi-steady aerodynamics (see Appendix), that vibrations in the rotor plane (edgewise) are less damped by the air flow than those out of the rotor plane (flapwise). Another important role of the structural dynamics is the *structural damping* of the blade. For example, if the first edgewise mode of a blade has a negative aerodynamic damping

* Correspondence to: M. H. Hansen, Wind Energy Department, Risø National Laboratory, PO Box 49, DK-4000 Roskilde, Denmark. E-mail: morten.hansen@risoe.dk
Contract/grant sponsor: Danish Energy Agency; Contract/grant number: ENS 1363/00-0006.

Published online 7 February 2003

Received 20 August 2002
Revised 5 November 2002
Accepted 12 November 2002

at some wind speeds, then it may be possible to avoid an instability by adding sufficient structural damping to the blade, or a distinct vibration damper.[10] Thus, besides the aerodynamic issue, it is necessary to consider the mode shapes and their structural damping when designing a new blade.

Another issue of stall-induced vibrations is the interaction of the blades with the remaining wind turbine. A numerical simulation of a turbine using the aeroelastic code HAWC[11] showed that, by stiffening the support of the rotor (shaft and nacelle), undamped edgewise blade vibrations could be avoided.[7] This observation may be related to an observation made by Thomsen *et al.*[1] They have developed an experimental method for estimating the total damping of a wind turbine during operation. Figure 1 shows the results of their experiments with a stall-controlled Bonus 600 kW wind turbine. The observation is that the forward rotor whirling mode associated with edgewise blade vibrations is more damped than the backward rotor whirling mode. The structural damping of these two modes is assumed to be the same, because their natural frequencies and mode shapes are almost identical; the difference in total damping is therefore a difference in aerodynamic damping.

In this article it is suggested that the dependence of aerodynamic damping on whirl direction and rotor support stiffness can be explained by analysing the turbine mode shapes. It is shown how a theoretical modal analysis can be performed for a rotating turbine based on the so-called *multi-blade co-ordinate transformation*.[12,13] For the particular 600 kW turbine it is shown that the blades vibrate more out of the rotor plane in the forward edgewise whirling mode than in the backward edgewise whirling mode. This observation can explain the measured difference in aerodynamic damping for the two whirling modes, because the direction of blade vibration with respect to the rotor plane is important for the aerodynamic damping in stall. It is suggested that, using the modal analysis, the design of wind turbines can be tailored to increase the blade vibration out of the rotor plane for all modes, and thereby increase the aerodynamic damping of stall-regulated turbines.

The next section describes the model and method for modal analysis of rotating turbines. The modal analysis of the 600 kW turbine is then presented, followed by a section on the measured differences in aerodynamic damping and the optimization of its dynamical behaviour.

Model and Method

A linear model of a three-bladed wind turbine is needed for the modal analysis. It must qualitatively describe the dynamics of the turbine up to the second tilt/yaw modes in order to study the phenomena mentioned above. Blade torsion is not included in the analysis, because the corresponding natural frequencies are several times higher than the dynamics of interest.

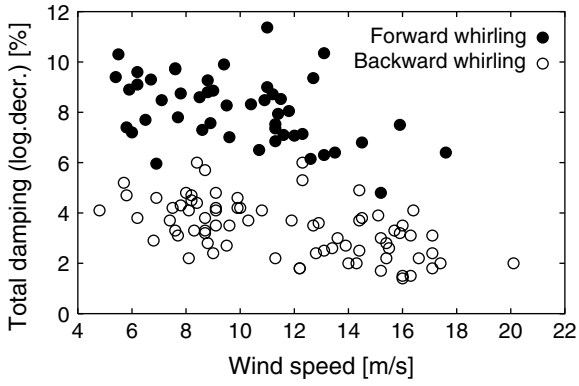

Figure 1. Total damping of the forward and backward edgewise whirling modes of the Bonus 600 kW estimated by Thomsen et al.[1]

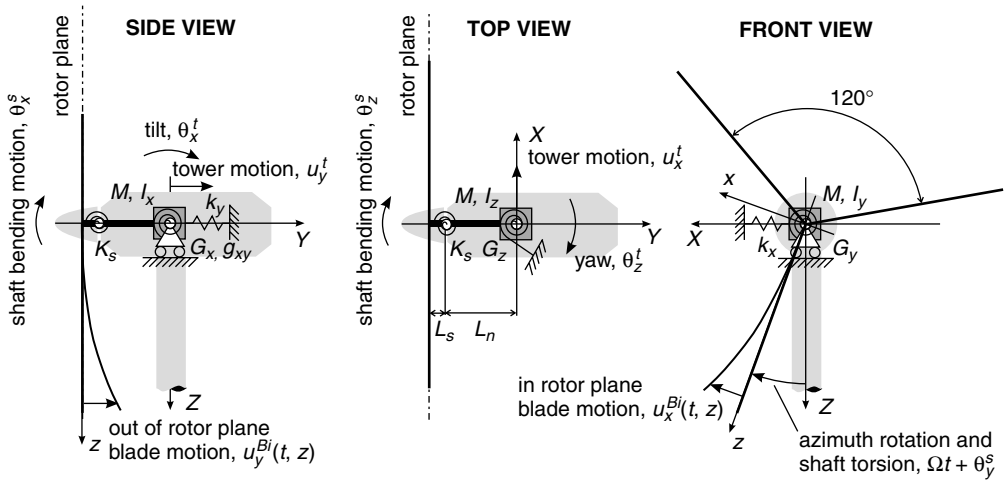

Figure 2. Simplified structural model of a wind turbine

Equations of Motion

A schema of the structural model is shown in Figure 2. The motion of the nacelle and tower is described by seven degrees of freedom (DOFs). The nacelle can translate in the two horizontal directions, described in the *ground fixed frame* (X, Y, Z) by u_x^{t} (lateral) and u_y^{t} (longitudinal), and can *tilt* and *yaw* about the tower top, described by the angles θ_x^{t} and θ_z^{t} respectively. The rotor can rotate out of its plane owing to bending of the shaft, described by the angles θ_x^{s} and θ_z^{s} defined in the co-rotating frame of blade number 1. Finally, the torsion of the shaft and drive-train is described by the angle θ_y^{s}.

The motions of the blades are described by a modal expansion defined in their own co-rotating frames (x, y, z), where the z-axis is the blade axis and the y-axis at rest coincides with the Y-axis. The in- and out-of-rotor-plane motions of blade number i are given by

$$u_x^{\mathrm{B}_i}(t, z) = \sum_{n=1}^{N} q_{i,n}(t)\Phi_n^x(z), \qquad u_y^{\mathrm{B}_i}(t, z) = \sum_{n=1}^{N} q_{i,n}(t)\Phi_n^y(z) \tag{1}$$

where $q_{i,n}$ are *modal blade co-ordinates* describing the contents of mode number n in the motion of blade number i, and Φ_n^x and Φ_n^y are the mode shape functions. These shape functions can be obtained numerically or experimentally.

For the derivation of the inertia forces it is assumed that the centre of mass (CM) for the undeformed blade lies along the z-axis. A vector in the blade frame (x, y, z) from the rotor centre to the CM at radius z is therefore given by

$$\mathbf{r}_i^{\mathrm{B}} = \sum_{n=1}^{N} \{\Phi_n^x(z), \Phi_n^y(z), z\}^{\mathrm{T}} q_{i,n}(t) \tag{2}$$

In the ground fixed frame (X, Y, Z) the motion of the CM at radius z on blade number i becomes

$$\mathbf{r}_i = \mathbf{r}_{\mathrm{t}} + \mathbf{T}_{\mathrm{t}}[\mathbf{r}_{\mathrm{ts}} + \mathbf{T}_{\mathrm{a}}\mathbf{T}_{\mathrm{s}}(\mathbf{r}_{\mathrm{sh}} + \mathbf{T}_{\mathrm{B}_i}\mathbf{r}_i^{\mathrm{B}})] \tag{3}$$

where $\mathbf{r}_{\mathrm{t}} = \{u_x^{\mathrm{t}}, u_y^{\mathrm{t}}, 0\}^{\mathrm{T}}$ is a vector from the origin to the tower top, $\mathbf{r}_{\mathrm{ts}} = \{0, -L_{\mathrm{n}}, 0\}^{\mathrm{T}}$ is a vector from the tower top to the bending point on the shaft in nacelle co-ordinates, and $\mathbf{r}_{\mathrm{sh}} = \{0, -L_{\mathrm{s}}, 0\}^{\mathrm{T}}$ is a vector from this point to the rotor centre in rotor co-ordinates. The transformation matrices $\mathbf{T}_{\mathrm{a}}$ and $\mathbf{T}_{\mathrm{B}_i}$ handling the azimuth

rotations are written as

$$\mathbf{T}_{\mathrm{B}_i} = \begin{bmatrix} \cos\left[\frac{2}{3}\pi(i-1)\right] & 0 & \sin\left[\frac{2}{3}\pi(i-1)\right] \\ 0 & 1 & 0 \\ -\sin\left[\frac{2}{3}\pi(i-1)\right] & 0 & \cos\left[\frac{2}{3}\pi(i-1)\right] \end{bmatrix}$$
$$\mathbf{T}_{\mathrm{a}} = \begin{bmatrix} \cos(\Omega t + \theta_y^{\mathrm{s}}) & 0 & \sin(\Omega t + \theta_y^{\mathrm{s}}) \\ 0 & 1 & 0 \\ -\sin(\Omega t + \theta_y^{\mathrm{s}}) & 0 & \cos(\Omega t + \theta_y^{\mathrm{s}}) \end{bmatrix} \tag{4}$$

where Ω is the rotation speed. It is assumed that all rotations of the tower top and hub are small ($\theta_x^{\mathrm{t}}, \theta_z^{\mathrm{t}}, \theta_x^{\mathrm{s}}, \theta_z^{\mathrm{s}} << 1$), whereby the remaining transformation matrices of equation (3) become

$$\mathbf{T}_{\mathrm{s}} = \begin{bmatrix} 1 & -\theta_z^{\mathrm{s}} & 0 \\ \theta_z^{\mathrm{s}} & 1 & -\theta_x^{\mathrm{s}} \\ 0 & \theta_x^{\mathrm{s}} & 1 \end{bmatrix}, \quad \mathbf{T}_{\mathrm{t}} = \begin{bmatrix} 1 & -\theta_z^{\mathrm{t}} & 0 \\ \theta_z^{\mathrm{t}} & 1 & -\theta_x^{\mathrm{t}} \\ 0 & \theta_x^{\mathrm{t}} & 1 \end{bmatrix} \tag{5}$$

where $\mathbf{T}_{\mathrm{s}}$ handles the transformation from rotor to nacelle co-ordinates due to shaft bending, and $\mathbf{T}_{\mathrm{t}}$ handles the transformation from nacelle co-ordinates to the ground fixed frame due to tilt and yaw.

The total kinetic energy of the wind turbine in this model can now be derived as

$$T = \frac{1}{2}\left(M(\dot{u}_x^{\mathrm{t}^2} + \dot{u}_y^{\mathrm{t}^2}) + I_x\dot{\theta}_x^{\mathrm{t}^2} + I_z\dot{\theta}_z^{\mathrm{t}^2} + I_y\dot{\theta}_y^{\mathrm{s}^2} + \sum_{i=1}^{3}\int_0^R m(z)|\dot{\mathbf{r}}_i|^2 \mathrm{d}z \right) \tag{6}$$

where $\dot{(\,)} \equiv \partial/\partial t$ denotes the time derivative, M is the total mass of the nacelle (and a part of the tower), I_x and I_z are the rotational inertias of the nacelle about the tilt and yaw axes respectively, I_y is the rotational inertia of the shaft and drive-train, R is the length of the blades including the hub and root extension, and $m(z)$ is the mass per unit length of the entire blade–root–hub assembly.

It is assumed that there is an elastic stiffness coupling between the nacelle tilt θ_x^{t} and the longitudinal tower motion u_y^{t}, whereby the potential energy is defined as

$$V = \frac{1}{2}\left[k_x u_x^{\mathrm{t}^2} + k_y u_y^{\mathrm{t}^2} + g_{xy} u_y^{\mathrm{t}} \theta_x^{\mathrm{t}} + G_x \theta_x^{\mathrm{t}^2} + G_z \theta_z^{\mathrm{t}^2} \right.$$
$$\left. + K_{\mathrm{s}}(\theta_x^{\mathrm{s}2} + \theta_z^{\mathrm{s}^2}) + G_y \theta_y^{\mathrm{s}^2} + \sum_{i=1}^{3}\left(\sum_{n=1}^{N} k_n q_{i,n}^2 + V_{\mathrm{c},i} \right) \right] \tag{7}$$

where k_x and k_y are the translational stiffnesses of the tower at its top, g_{xy} is the coupling stiffness between nacelle tilt and longitudinal tower motion, G_x and G_z are the rotational stiffnesses of the tower at its top, K_{s} is the bending stiffness of the shaft, and G_y is the torsional stiffness of the shaft and drive-train. The *modal stiffness* k_n is defined as $k_n \equiv \omega_n^2 M_n$, where ω_n is the natural frequency of blade mode number n, and M_n is the *modal mass*, $M_n \equiv \int_0^R m(z)(\Phi_n^{x^2} + \Phi_n^{y^2})\mathrm{d}z$.

The potential energy term $V_{\mathrm{c},i}$ is added for modelling of the centrifugal stiffening effect. The tensile force in the blade due to centrifugal body forces is $\Omega^2 \int_z^R m(\zeta)\zeta \mathrm{d}\zeta$, and the additional potential energy due to the centrifugal body forces can be approximated by

$$V_{\mathrm{c},i} = \frac{1}{2}\Omega^2 \int_0^R \left[\left(\sum_{n=1}^{N} q_{i,n} \frac{\mathrm{d}\Phi_n^x}{\mathrm{d}z} \right)^2 + \left(\sum_{n=1}^{N} q_{i,n} \frac{\mathrm{d}\Phi_n^y}{\mathrm{d}z} \right)^2 \right] \int_z^R m(\zeta)\zeta \mathrm{d}\zeta \mathrm{d}z \tag{8}$$

where it is assumed that rotations of the blade cross-sections due to bending are small.

The blade and tower/nacelle co-ordinates are collected in a state vector

$$\mathbf{x} = \{q_{1,1}, \ldots, q_{1,N}, q_{2,1}, \ldots, q_{2,N}, q_{3,1}, \ldots, q_{3,N}, \theta_x^{\mathrm{s}}, \theta_z^{\mathrm{s}}, u_x^{\mathrm{t}}, u_y^{\mathrm{t}}, \theta_x^{\mathrm{t}}, \theta_z^{\mathrm{t}}, \theta_y^{\mathrm{s}}\}^{\mathrm{T}} \tag{9}$$

and Lagrange's equations are derived from the Lagrangian $L = T - V$. After linearization about the undeformed state by assuming small amplitudes of the co-ordinates, $x_j << 1$, the equations of motion can be written in the form

$$\mathbf{M}(t)\ddot{\mathbf{x}} + \mathbf{C}(t)\dot{\mathbf{x}} + \mathbf{K}(t)\mathbf{x} = \mathbf{0} \tag{10}$$

Where **M**, **C** and **K** are the mass, gyroscopic and stiffness matrices respectively. All three matrices are time-dependent, containing harmonic terms with period $T = 2\pi/\Omega$.

Note that structural damping is neglected in this simplified wind turbine model. The lower-order modes of interest to this study are low damped, thus structural damping has practically no effect on their mode shapes. For studies of resonance phenomena and stability it would be necessary to include the structural damping.[14]

The equations of motion (10) have a form that is general for linear structural models of wind turbines. The periodic terms arising from the azimuthal rotation prevent a direct derivation of the natural frequencies and mode shapes from an eigenvalue problem. Still, the mathematical approach of using *Floquet theory* should be avoided, because there is a more physically comprehensive way to set up an eigenvalue problem.

Multi-blade Co-ordinate Transformation

The use of *multi-blade co-ordinates*, or *Fourier co-ordinates*, for bladed rotors[12,13] is a method to describe the motions of individual blades in the same co-ordinate system as the structure supporting the rotor, whereby the periodic terms in the governing equations are eliminated. The fundamental assumption of this method is that the rotor is *isotropic*, i.e. all blades are identical, identically pitched and symmetrically mounted on the hub.

In the wind turbine model given by equation (10), the motion of the tower/nacelle is described in the ground fixed frame, while the shaft bending is described in rotating shaft co-ordinates, and the motions of the three blades are described in their own co-rotating frames. The shaft bending can easily be described in the ground fixed frame by a co-ordinate transformation with respect to the azimuth angle. The transformation of the blade co-ordinates into the ground fixed frame can be done by the multi-blade co-ordinate transformation, which is defined by

$$q_{i,n} = a_{0,n} + a_{1,n}\cos\psi_i + b_{1,n}\sin\psi_i \tag{11}$$

where $\psi_i = \Omega t + \frac{2}{3}\pi(i-1)$ is the azimuth angle to blade number i (without shaft torsion) measured from the Z-axis.

The three multi-blade co-ordinates $a_{0,n}$, $a_{1,n}$ and $b_{1,n}$ replace the three blade co-ordinates $q_{1,n}$, $q_{2,n}$ and $q_{3,n}$. To see that the multi-blade co-ordinates describe the rotor motion in the ground fixed frame, assume that blade mode n is the first flapwise bending mode. Then $a_{0,n}$ describes a simultaneous flapwise deflection of all three blades, while $a_{1,n}$ and $b_{1,n}$ describe tilt and yaw motions respectively.

The multi-blade transformation of the state vector **x** can be represented by

$$\mathbf{x} = \mathbf{B}(t)\mathbf{z} \tag{12}$$

where the state vector **z** containing the multi-blade co-ordinates is

$$\mathbf{z} = \{a_{0,1}, \ldots, a_{0,N}, a_{1,1}, \ldots, a_{1,N}, b_{1,1}, \ldots, b_{1,N}, \theta_X^{\mathrm{s}}, \theta_Z^{\mathrm{s}}, u_x^{\mathrm{t}}, u_y^{\mathrm{t}}, \theta_x^{\mathrm{t}}, \theta_z^{\mathrm{t}}, \theta_y^{\mathrm{s}}\}^{\mathrm{T}} \tag{13}$$

and the transformation matrix is

$$\mathbf{B} \equiv \begin{bmatrix} \mathbf{I}_N & \mathbf{I}_N \cos\psi_1 & \mathbf{I}_N \sin\psi_1 & \mathbf{0} & \mathbf{0} & \mathbf{0} \\ \mathbf{I}_N & \mathbf{I}_N \cos\psi_2 & \mathbf{I}_N \sin\psi_2 & \mathbf{0} & \mathbf{0} & \mathbf{0} \\ \mathbf{I}_N & \mathbf{I}_N \cos\psi_3 & \mathbf{I}_N \sin\psi_3 & \mathbf{0} & \mathbf{0} & \mathbf{0} \\ \mathbf{0} & \mathbf{0} & \mathbf{0} & \cos\Omega t & -\sin\Omega t & \mathbf{0} \\ \mathbf{0} & \mathbf{0} & \mathbf{0} & \sin\Omega t & \cos\Omega t & \mathbf{0} \\ \mathbf{0} & \mathbf{0} & \mathbf{0} & \mathbf{0} & \mathbf{0} & \mathbf{I}_5 \end{bmatrix} \tag{14}$$

where $\mathbf{I}_N$ is the identity matrix of size $N \times N$. The matrix $\mathbf{B}$ has the following properties:

$$\begin{aligned} \mathbf{B}^{-1}\dot{\mathbf{B}} &= \begin{bmatrix} \mathbf{0} & \mathbf{0} & \mathbf{0} & \mathbf{0} & \mathbf{0} & \mathbf{0} \\ \mathbf{0} & \mathbf{0} & \Omega\mathbf{I}_N & \mathbf{0} & \mathbf{0} & \mathbf{0} \\ \mathbf{0} & -\Omega\mathbf{I}_N & \mathbf{0} & \mathbf{0} & \mathbf{0} & \mathbf{0} \\ \mathbf{0} & \mathbf{0} & \mathbf{0} & 0 & -\Omega & \mathbf{0} \\ \mathbf{0} & \mathbf{0} & \mathbf{0} & \Omega & 0 & \mathbf{0} \\ \mathbf{0} & \mathbf{0} & \mathbf{0} & \mathbf{0} & \mathbf{0} & \mathbf{0} \end{bmatrix} \equiv \mathbf{R} \\ \mathbf{B}^{-1} &= \boldsymbol{\mu}\mathbf{B}^{\mathrm{T}}, \quad \boldsymbol{\mu} = \begin{bmatrix} \frac{1}{3}\mathbf{I}_N & \mathbf{0} & \mathbf{0} & \mathbf{0} \\ \mathbf{0} & \frac{2}{3}\mathbf{I}_N & \mathbf{0} & \mathbf{0} \\ \mathbf{0} & \mathbf{0} & \frac{1}{3}\mathbf{I}_N & \mathbf{0} \\ \mathbf{0} & \mathbf{0} & \mathbf{0} & \mathbf{I}_7 \end{bmatrix} \end{aligned} \tag{15}$$

which shows that $\dot{\mathbf{B}} = \mathbf{BR}$ and $\ddot{\mathbf{B}} = \mathbf{BR}^2$. A transformation of equation (10) into the multi-blade co-ordinates (12) yields

$$\mathbf{M}_{\mathrm{B}}\ddot{\mathbf{z}} + (2\mathbf{M}_{\mathrm{B}}\mathbf{R} + \mathbf{C}_{\mathrm{B}})\dot{\mathbf{z}} + (\mathbf{M}_{\mathrm{B}}\mathbf{R}^2 + \mathbf{C}_{\mathrm{B}}\mathbf{R} + \mathbf{K}_{\mathrm{B}})\mathbf{z} = 0 \tag{16}$$

where $\mathbf{M}_{\mathrm{B}} \equiv \boldsymbol{\mu}\mathbf{B}^{\mathrm{T}}\mathbf{M}\mathbf{B}$, $\mathbf{C}_{\mathrm{B}} \equiv \boldsymbol{\mu}\mathbf{B}^{\mathrm{T}}\mathbf{C}\mathbf{B}$ and $\mathbf{K}_{\mathrm{B}} \equiv \boldsymbol{\mu}\mathbf{B}^{\mathrm{T}}\mathbf{K}\mathbf{B}$ are the transformed system matrices. If the rotor is isotropic, these matrices are *constant*, i.e. the transformed equations of motion in the multi-blade co-ordinates (16) contain no periodic terms. It is therefore possible to define an eigenvalue problem that gives the natural frequencies and mode shapes of the wind turbine with a rotating rotor.

Eigenvalue Problem and Solution

A substitution of the solution $\mathbf{z} = \mathbf{z}_k \mathrm{e}^{\lambda_k t}$ into (16) yields an eigenvalue problem that determines the complex eigenvalues $\lambda_k \equiv \sigma_k + \mathrm{i}\omega_k$ ($\mathrm{i} \equiv \sqrt{-1}$) and complex eigenvectors $\mathbf{z}_k$ of mode number k.

Inserting the solution $\mathbf{z} = \mathbf{z}_k \mathrm{e}^{\lambda_k t}$ into (12), the blade co-ordinate $q_{i,n}$ for the modal content of blade mode number n in the motion of blade number i becomes

$$\begin{aligned} q_{i,n,k} = {} & A^0_{n,k}\mathrm{e}^{\sigma_k t}\cos(\omega_k t + \phi^0_{\beta,k}) \\ & + \tfrac{1}{2}A^{\mathrm{BW}}_{n,k}\mathrm{e}^{\sigma_k t}\cos[(\omega_k + \Omega)t + \tfrac{2}{3}\pi(i-1) + \phi^{\mathrm{BW}}_{n,k}] \\ & + \tfrac{1}{2}A^{\mathrm{FW}}_{n,k}\mathrm{e}^{\sigma_k t}\cos[(\omega_k - \Omega)t - \tfrac{2}{3}\pi(i-1) + \phi^{\mathrm{FW}}_{n,k}] \end{aligned} \tag{17}$$

where the amplitudes and phases are determined by the complex eigenvectors

$$\begin{aligned} A^0_{n,k} &= \tfrac{1}{2}\sqrt{\mathrm{Re}\{a_{0,n,k}\}^2 + \mathrm{Im}\{a_{0,n,k}\}^2} \\ A^{\mathrm{BW}}_{n,k} &= \tfrac{1}{2}\sqrt{(\mathrm{Re}\{b_{1,n,k}\} - \mathrm{Im}\{a_{1,n,k}\})^2 + (\mathrm{Im}\{b_{1,n,k}\} + \mathrm{Re}\{a_{1,n,k}\})^2} \\ A^{\mathrm{FW}}_{n,k} &= \tfrac{1}{2}\sqrt{(\mathrm{Re}\{b_{1,n,k}\} + \mathrm{Im}\{a_{1,n,k}\})^2 + (\mathrm{Re}\{a_{1,n,k}\} - \mathrm{Im}\{b_{1,n,k}\})^2} \end{aligned} \tag{18}$$

and

$$\begin{aligned}\phi^{0}_{n,k} &= \tan^{-1}(\mathrm{Im}\{a_{0,n,k}\}/\mathrm{Re}\{a_{0,n,k}\})\\ \phi^{\mathrm{BW}}_{n,k} &= \tan^{-1}[(\mathrm{Im}\{a_{1,n,k}\} - \mathrm{Re}\{b_{1,n,k}\})/(\mathrm{Im}\{b_{1,n,k}\} + \mathrm{Re}\{a_{1,n,k}\})]\\ \phi^{\mathrm{FW}}_{n,k} &= \tan^{-1}[(\mathrm{Re}\{b_{1,n,k}\} + \mathrm{Im}\{a_{1,n,k}\})/(\mathrm{Re}\{a_{1,n,k}\} - \mathrm{Im}\{b_{1,n,k}\})]\end{aligned} \tag{19}$$

Equation (17) shows that the motion of blade number i for mode number k consists of three components: a symmetric component where all blades deflect simultaneously in blade mode number n with the amplitude $A^{0}_{n,k}$, and two asymmetric components where the blades deflect with phase shifts of $T/3$ and the amplitudes $A^{\mathrm{BW}}_{n,k}$ and $A^{\mathrm{FW}}_{n,k}$ respectively. As indicated by the superscripts, the asymmetric components represent *backward* and *forward rotor whirling*. The direction of the whirl is determined by the sign of the blade-dependent phase shifts $\frac{2}{3}\pi(i-1)$.

The frequency of the symmetric component is ω_k, while the frequencies of the whirling components are shifted by $\pm\Omega$. The reason for these frequency shifts is that the natural frequency ω_k is given in the ground fixed frame. An observer on the tower top (in the ground fixed frame) will measure the natural frequency ω_k for all three modes. An observer on a blade will also measure the frequency ω_k for symmetric modes, but for backward and forward whirling modes the same observer will measure the frequencies $\omega_k + \Omega$ and $\omega_k - \Omega$ respectively.

The damping of the turbine modes is described by the term $\mathrm{e}^{\sigma_k t}$; the modal damping factor σ_k determines the exponential decay, or growth, of amplitude for a vibration in mode number k. The computation of the damping factors can therefore be used for stability analyses, e.g. the flutter analysis of a wind turbine.[15]

Modal Analysis of the Experimental 600 kW Turbine

This section contains derivations of the natural frequencies and mode shapes of the Bonus 600 kW wind turbine used in the experiments by Thomsen *et al.*[1] A *Campbell diagram* shows the natural frequencies of the turbine as a function of rotation speed. A mode identification study shows that some of the corresponding mode shapes change dramatically as the rotation speed is changed, owing to modal interactions.

Model Parameters

The Bonus 600 kW (Mk III C) wind turbine with its LM 19·1 m blades has a rotor radius of 22 m with hub and root extension. For this study, two blade modes are chosen ($N = 2$): first flapwise and first edgewise bending modes for the non-rotating blade. The shape functions Φ^{x}_{n} and Φ^{y}_{n} of the entire blade–root–hub assembly are obtained from curve fits to the results of a finite element model (see Figure 3). The functions are normalized so that the associated modal masses are one. The natural frequencies of the flapwise and edgewise blade modes (as measured in a test stand with the hub and root extension) are 1·70 and 2·94 Hz respectively.

The remaining model parameters are obtained by tuning the natural frequencies of the stationary turbine ($\Omega \equiv 0$) to the frequencies measured for the particular experimental turbine. The turbine is operating at a speed of about 27·4 rpm ($\Omega \approx 2{\cdot}87$ rad s^{-1}).

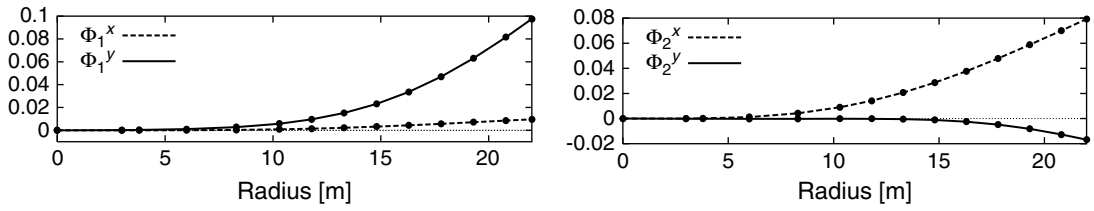

Figure 3. Mode shape functions for the blade–root–hub assembly: first flapwise mode (left) and first edgewise mode (right). The functions are curve fits to the points obtained from a finite element model with Timoshenko beam elements

Table I. Modelled and measured natural frequencies of the lowest 10 modes of the stationary turbine

Mode no.	Name	Modelled frequency (Hz)	Measured frequency (Hz)
1	1st shaft torsion	0·57	0·56
2	1st longitudinal tower bending	0·73	0·73
3	1st lateral tower bending	0·78	0·80
4	1st yawing flap	1·24	1·20
5	1st tilting flap	1·48	1·50
6	1st symmetric flap	1·76	1·76
7	1st vertical edgewise	2·85	2·90
8	1st horizontal edgewise	2·95	
9	2nd yawing flap	3·43	3·60
10	2nd tilting flap	3·74	

Natural Frequencies and Mode Shapes

Modelled and measured natural frequencies of the 10 lowest modes of the stationary turbine are listed in Table I. The measured frequencies are obtained from identification of peaks in frequency responses. For the mode pairs 7/8 and 9/10 it is only possible to identify a single response peak.

A comparison of modelled and measured frequencies leads to the assumption that the model is sufficiently tuned to the experimental turbine. The naming of the 10 lowest modes is based on animations of their mode shapes and the measured frequency responses. The sequence of modes is typical for a turbine of this size, with the exception that the 1st shaft torsion may be higher than the tower bending modes. The longitudinal tower bending always lies slightly lower than the lateral tower bending mode, because it contains some tilting of the rotor, which has a large inertia.

Modes 4 and 5 are the 1st tilt/yaw modes involving the flapwise blade mode. The yaw mode most often lies lower than the tilt mode, because towers are stiffer in tilt than in yaw. The sixth mode is the 1st symmetrical flap mode, where the blades vibrate simultaneously in the flapwise blade mode in counter-phase with a longitudinal tower vibration. This coupling causes the symmetric flap frequency to lie slightly above the frequency of the flapwise blade mode.

Modes 7 and 8 involve the edgewise blade mode, and their frequencies are close to the edgewise blade frequency of 2·94 Hz (with an average slightly below). In both modes the blades vibrate edgewise against each other so that they cancel out the torsional moment at the rotor centre. The two modes differ in the direction of the reactive force at the rotor centre, as indicated by their names: 1st vertical and 1st horizontal edgewise mode. The sequence of these two modes is given by the vertical and horizontal stiffness of the rotor support.

The last two modes listed in Table I are the 2nd tilt/yaw modes, where the rotor blades are tilting and yawing in counter-phase with the tilt and yaw of the nacelle. Again the yaw mode lies below the tilt mode because of the lower yaw than tilt stiffness of the tower.

Figure 4 shows how the natural frequencies ω_k of these 10 lowest modes change with the rotation speed Ω from standstill to the operation speed. The natural frequencies of the tower bending modes and the shaft torsion mode are constant with rotation speed. The frequency of the symmetric flap mode increases owing to centrifugal stiffening of flapwise bending. The natural frequencies of the asymmetric rotor modes change with rotation speed owing to gyroscopic effects.

The naming of the modes at operation listed in the table in Figure 4 requires some introduction. All pairs of asymmetric rotor modes at standstill (modes 4/5, 7/8 and 9/10) become pairs of rotor whirling modes owing to the rotation, e.g. the 1st tilt/yaw modes become the *1st flapwise whirling modes*. The frequencies of the backward whirling (BW) modes decrease with rotation speed, whereas the frequencies of the forward whirling (FW) modes increase with rotation speed.

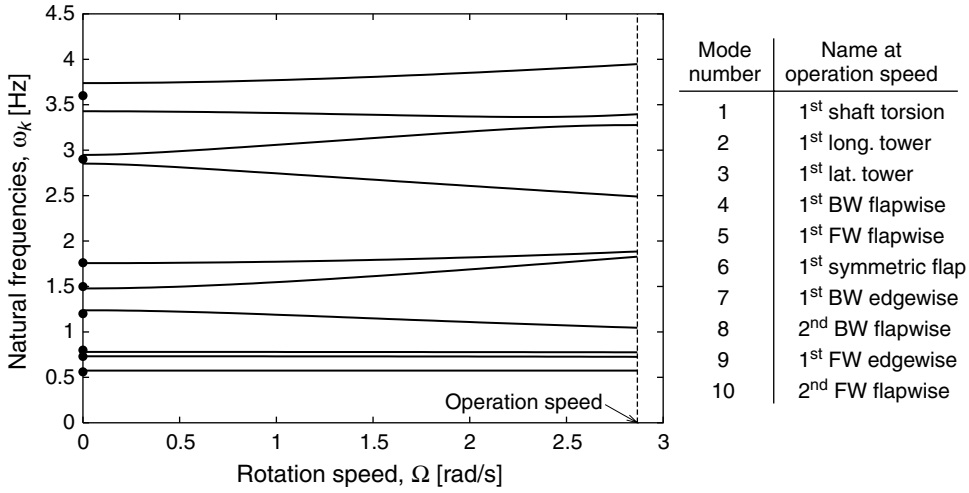

Figure 4. Campbell diagram: natural frequencies as a function of rotation speed of the rotor. The points denote the measured natural frequencies for the turbine at standstill

This splitting of the natural frequencies of a whirling mode pair is related to the co-ordinate system of observation through gyroscopic effects. The natural frequencies ω_k in Figure 4 are observed from the ground fixed frame. Equation (17) shows that in a co-rotating blade frame the frequency of a symmetric rotor mode remains ω_k, whereas the frequencies of BW and FW modes become $\omega_k + \Omega$ and $\omega_k - \Omega$ respectively. If only blade mode number n is involved in the whirling modes, their frequencies split in the ground fixed frame about the natural frequency ω_n of this blade mode. In this ideal case the observer on the blade will measure the same frequency $\omega_n = \omega_k^{\mathrm{BW}} + \Omega = \omega_k^{\mathrm{FW}} - \Omega$ for both the BW and FW modes.

This ideal condition is affected by structural asymmetry of the turbine and coupling of blade modes in the turbine modes. Such modal interactions may occur when the natural frequencies of two turbine modes come close. Figure 4 shows that the frequencies of the 1st FW edgewise mode (mode 8) and the 2nd BW flapwise mode (mode 9) become close at about $\Omega = 2{\cdot}5$ rad s^{-1}. These two modes interact, which can be shown by the flapwise and edgewise whirling components in their mode shapes.

Figure 5 shows the FW and BW components of the flapwise and edgewise blade modes in modes 7–10. These whirling components are computed from the eigenvectors in multi-blade co-ordinates using equation (18). The dominating amplitudes for modes 7 and 10 show that these modes are respectively a BW edgewise and an FW flapwise mode. However, there are no dominant modal amplitude for modes 8 and 9 over the whole range of rotation speeds. It seems that these modes interchange mode shapes: mode 8 can be defined as an FW edgewise mode and mode 9 as a BW flapwise mode at rotation speeds below 2·5 rad s^{-1}, and *vice versa* above this speed.

At the operation speed, mode 9 must be characterized as the 1st FW edgewise mode with some content of flapwise whirling. This content is now suggested to explain the observed difference in aerodynamic damping of the BW and FW edgewise modes (modes 7 and 9).

Why the Measured Difference in Aerodynamic Damping?

Thomsen *et al.*[1] have estimated the total damping of the two edgewise whirling modes (see Figure 1). The results show that the FW edgewise mode (mode 9) is more damped than the BW edgewise mode (mode 7). The structural damping of these two modes is assumed to be the same, because their natural frequencies and mode shapes are almost identical. Thus the difference in total damping is assumed to be caused by a difference in aerodynamic damping.

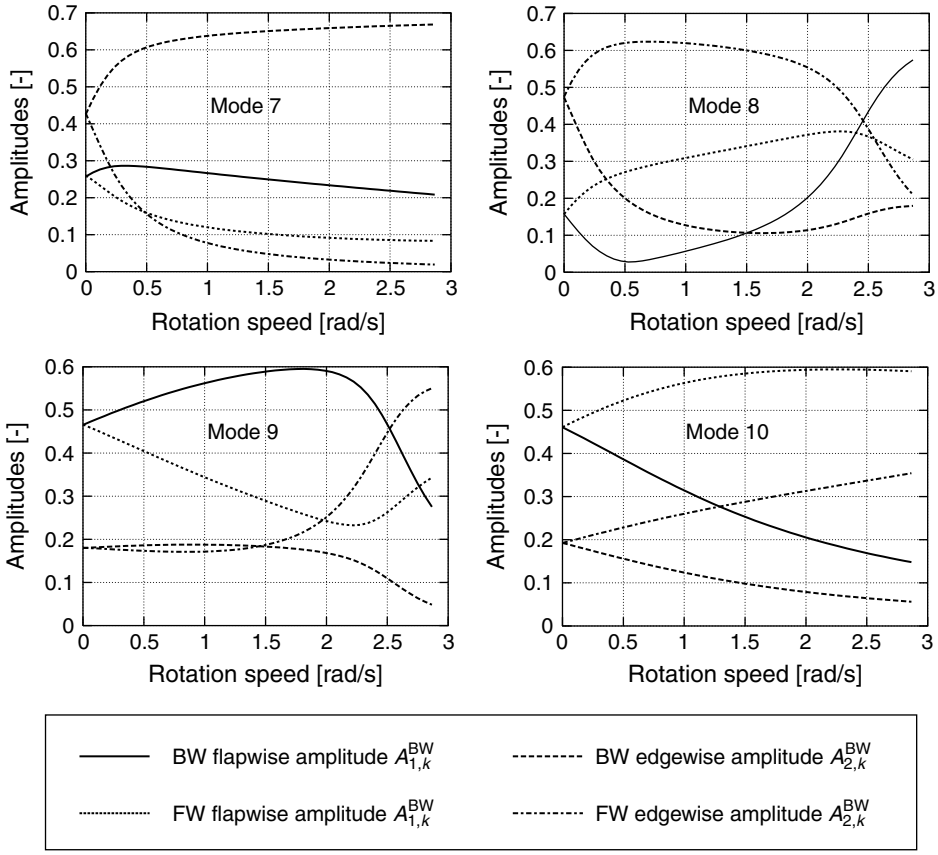

Figure 5. Flapwise and edgewise whirling components of the modal blade amplitudes for modes 7–10 computed from the eigenvectors using equation (18)

The aim of the experiment was to measure the damping of edgewise blade vibrations during turbine operation by exciting the corresponding turbine modes using an exciter mounted in the nacelle. The presented theoretical modal analysis of the turbine was not available for the experiment. The excitation of the edgewise whirling modes was therefore based on tuning the excitation frequency to obtain the maximum edgewise blade response. The two initial guesses, however, were based on the assumption that the ideal condition for frequency splitting existed, i.e. the excitation frequency should be the natural frequency of the edgewise blade mode plus or minus the operation speed (1P).

Figure 6 shows a zoom in the Campbell diagram (Figure 4) on the natural frequencies of modes 7–9, together with lines of the $\pm$1P splitting about the edgewise blade frequency (2·94 Hz). These lines intersect with the natural frequencies of modes 7 and 9 at the operation speed, showing that the initial guesses on the experimental excitation frequencies are close. However, the modal analysis has also shown that mode 9 is not a pure edgewise whirling mode; it has some flapwise component. This component affects the direction in which the blades are vibrating relative to the rotor plane.

Effective Direction of Blade Vibration

Figure 7 shows how the blade cross-section at 90% radius is moving in and out of the rotor plane during vibrations in the two edgewise whirling modes (modes 7 and 9). The motion of the cross-section includes the motion of the rotor support, i.e. the shaft and tower deformations add to the effective blade vibration. The traces show that the blades move more out of the rotor plane in the FW edgewise mode than in the

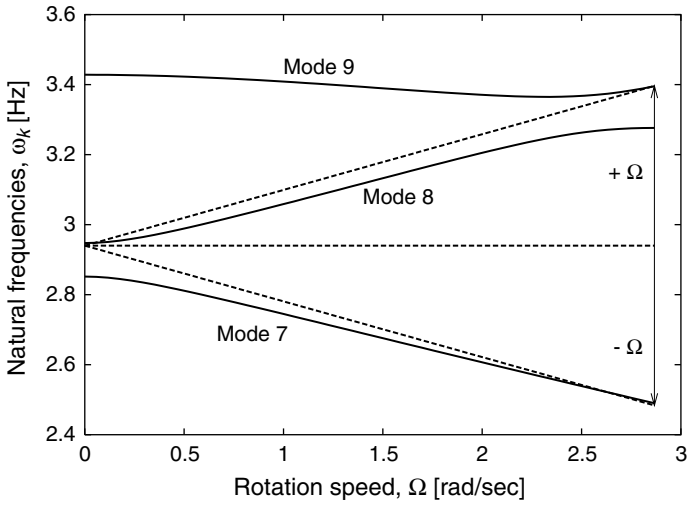

Figure 6. A zoom in the Campbell diagram (Figure 4) on the natural frequencies of modes 7–9. The broken lines show the ±Ω splitting about the edgewise blade frequency (2·94 Hz)

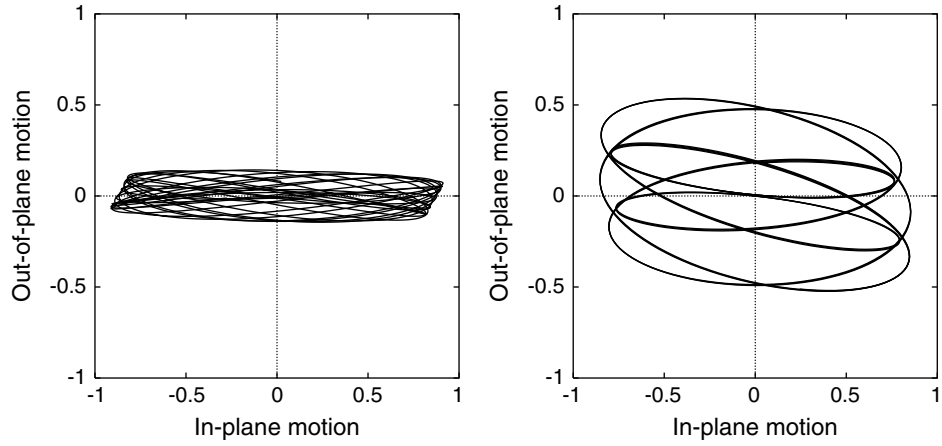

Figure 7. Motion of a blade cross-section at 90% radius for the 1st BW edgewise mode (left) and the 1st FW edgewise mode (right). The motion includes the tower and shaft deformations

BW edgewise mode. This difference in blade vibration for the two modes can explain why Thomsen *et al.* observed that the FW mode is more damped than the BW mode.

A quasi-steady aerodynamic analysis in the Appendix shows that the aerodynamic damping of a blade cross-section is lowest for vibrations close to the rotor plane. It is presumed in the analysis that the blade cross-section is performing a *small elliptical motion*, with the major axes being parallel and perpendicular to the rotor plane. This type of motion is assumed to characterize the qualitative pattern of the traces in Figure 7, except for a slight tilt of the major axes which originates from the direction of blade vibration for the edgewise blade mode (see Figure 3). An *effective direction of blade vibration* is defined for the elliptical motion of a blade cross-section as

$$\theta_{\text{eff}} = \tan^{-1}\left(\frac{\text{max. amplitude out of rotor plane}}{\text{max. amplitude in rotor plane}}\right) \tag{20}$$

Because the elliptical motion is assumed to have the major axes parallel and perpendicular to the rotor plane, the maximum amplitudes are positive, yielding $0^\circ < \theta_{\text{eff}} < 90^\circ$. Using this definition on the motion of the cross-section at 90% radius in Figure 7, it is found that $\theta_{\text{eff}} \approx 9^\circ$ and 30° for the 1st BW and FW edgewise modes respectively. Computations of θ_{eff} along the blade show that the entire blade is vibrating more out of the rotor plane in the 1st FW edgewise mode than in the 1st BW edgewise mode. Hence, based on quasi-steady aerodynamics, this behaviour can explain the measured difference in aerodynamic damping of these two modes.

Improved Modal Dynamics

The out-of-plane motion of the blades in the 1st FW edgewise mode is mainly due to a component of the flapwise blade mode through the previously described modal interaction with the 2nd BW flapwise mode (see Figure 5). The 1st BW edgewise mode is not interacting with a flapwise whirling mode; the blades are mainly vibrating in the edgewise blade mode (with the additional motion due to the tower and shaft deformations). Is it possible to add a flapwise component to the BW edgewise mode without removing the flapwise component in the FW edgewise mode, thereby increasing the overall aerodynamic damping of the turbine?

An example shows that such improvement of the modal dynamics of the Bonus 600 kW turbine may be possible. The natural frequency of the edgewise blade mode is chosen to be the design parameter in this optimization problem. Note that in reality an improved design must be the result of an integrated process towards a 'global optimum', where not only a single design parameter (the edgewise blade stiffness) is considered to achieve a single objective (the effective direction of blade vibration).

Figure 8 shows the effective directions of blade vibration defined by equation (20) at the 90% radius for modes 7–10 as function of the edgewise blade frequency. The modes are here named by their numbers, because their modal interactions prevent a unique mode identification over the entire range of design variation. These modes are all interesting, because they involve the edgewise blade mode. Shaft torsion and lateral tower bending modes also involve blade vibrations close to the rotor plane; however, the resulting low aerodynamic damping is compensated by high structural damping due to the generator slip of an asynchronous machine.

A local optimum is marked at an increase of 22% in the edgewise blade frequency, from 2·94 to 3·59 Hz. For this design the effective direction of blade vibration for mode 7 has tripled to approximately 27°. The effective direction of blade vibration has also increased for mode 8; however, the blades are now vibrating closer to the rotor plane in modes 9 and 10. In fact, mode 10 would be the most critical mode for higher edgewise blade frequencies.

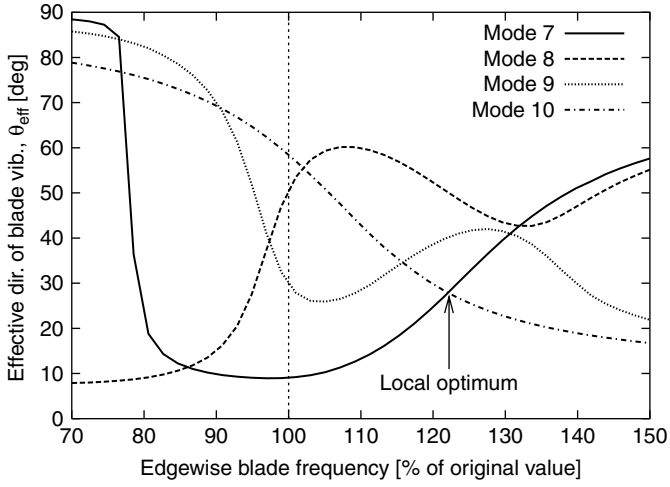

Figure 8. Effective directions of blade vibration at 90% radius with respect to the rotor plane for modes 7–10 as a function of the edgewise blade frequency

The improved design (with respect to the effective direction of blade vibration) uses the modal interaction with 2nd flapwise whirling modes to increase the flapwise component in the 1st edgewise whirling modes. It is not a coincidence that the optimal edgewise blade frequency is almost identical to the average frequency of the 2nd tilt and yaw modes at standstill (see Table I and Figure 4). Figure 9 shows a Campbell diagram for modes 7–10 of the improved turbine, together with the $\pm 1P$ splitting about the edgewise blade frequency. The ideal condition with a single blade mode involved in the rotor whirling mode is not present, and the modal interaction of edgewise and flapwise whirling is complete.

For this particular turbine it may be impossible to increase the edgewise blade frequency by 22%; however, by changing other design parameters, it may be possible to lower the frequencies of the 2nd flapwise whirling modes to obtain the desired modal interaction. A rule of thumb in structural design for maximum out-of-rotor-plane blade vibration can be formulated as: *Make sure the 1st edgewise blade frequency lies between the frequencies of the 2nd tilt and yaw modes*. Whether and how this design guideline can be followed will depend on the wind turbine.

Conclusion

A theoretical modal analysis of a three-bladed wind turbine shows that the blades cannot be considered as separate dynamic components of the turbine. Blade vibrations in the different modes of the turbine are strongly affected by the dynamics of the shaft, nacelle and tower. It is therefore necessary to consider the dynamics of the complete turbine when estimating the risk of stall-induced blade vibrations.

The analysis of a stall-controlled 600 kW turbine suggests why the forward and backward edgewise whirling modes have been observed to have different aerodynamic damping.[1] The explanation is a difference in the blade vibration for the two edgewise whirling modes. The forward whirling mode interacts with a flapwise whirling mode, whereby the blades vibrate more out of the rotor plane, yielding an increased aerodynamic damping.

Variations of the turbine design indicate that the structural dynamics of a wind turbine can be tailored to obtain a higher aerodynamic damping of its critical modes. A rule of thumb in structural design to lower the risk of stall-induced edgewise vibrations can be formulated as: *Make sure the 1st edgewise blade frequency*

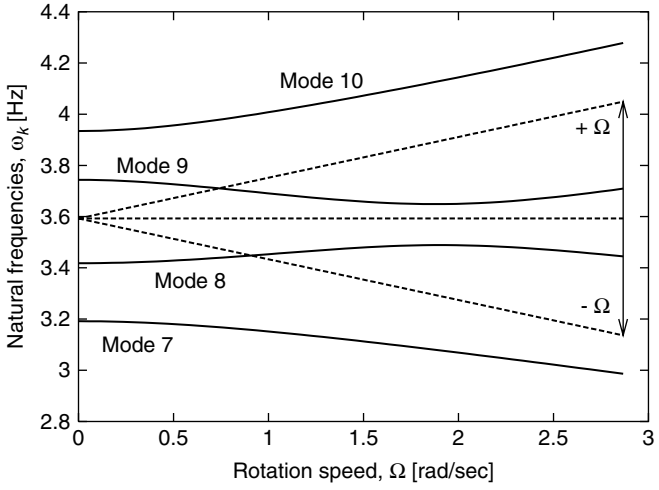

Figure 9. Natural frequencies of modes 7–10 for the improved turbine. The broken lines show the $\pm\Omega$ splitting about the new edgewise blade frequency of 3·59 Hz

lies between the frequencies of the 2nd tilt and yaw modes. Whether and how this design guideline can be followed will depend on the wind turbine.

Acknowledgements

This work was partly funded by the Danish Energy Agency under ENS 1363/00-0006, which is gratefully acknowledged. The author would also like to thank Kenneth Thomsen and Jørgen Thirstrup Petersen for their many invaluable discussions and suggestions.

Appendix: Aerodynamic Damping

This appendix deals with the aerodynamic damping of blade vibrations based on quasi-steady aerodynamics. Unsteady aerodynamic effects can be dominating when the blades operate in stall; however, the basic qualitative behaviour of the aerodynamic damping is assumed to be described by quasi-steady aerodynamics (see e.g. References 8 and 16 for details on *dynamic stall* effects).

The aim is to determine the aerodynamic damping of a vibrating blade cross-section. The cross-section is assumed to translate in and out of the rotor plane with the velocities $\dot{u}_x$ and $\dot{u}_y$ respectively, as shown in Figure 10. Torsional motion is neglected. The velocity triangle shows that the relative flow angle with respect to the rotor plane and the relative flow speed are

$$\phi = \tan^{-1}\left(\frac{V - \dot{u}_y}{r\Omega + \dot{u}_x}\right), \qquad W = \sqrt{(V - \dot{u}_y)^2 + (r\Omega + \dot{u}_x)^2} \tag{21}$$

where V is the wind speed, and the product of radius and rotation speed, $r\Omega$, is the steady tangential speed of the cross-section. Note that induced velocities from the wake behind the turbine are neglected, which has no qualitative influence on the derivations. The *angle of attack* is the difference between the relative flow angle and the twist of the cross-section: $\alpha = \phi - \theta$.

The assumption of quasi-steady conditions (neglecting *added mass* effects) means that the lift and drag on the cross-section can be written as

$$L(\dot{u}_x, \dot{u}_y) = \frac{1}{2}c\rho W^2 C_{\mathrm{L}}(\alpha), \quad D(\dot{u}_x, \dot{u}_y) = \frac{1}{2}c\rho W^2 C_{\mathrm{D}}(\alpha) \tag{22}$$

where c is the chord length, ρ is the air density, and C_{L} and C_{D} are the steady aerodynamic lift and drag coefficients given as functions of the angle of attack. The lift and drag forces are non-linear functions of the velocities $\dot{u}_x$ and $\dot{u}_y$ of the cross-section.

Assuming that these velocities are small compared with the steady flow velocities ($\dot{u}_x << r\Omega$ and $\dot{u}_y << V$), the aerodynamic forces (22) are linearized and projected onto the co-ordinate system of the rotor plane (x, y). The resulting linear quasi-steady aerodynamic forces can be written as

$$\mathrm{F} = \begin{Bmatrix} F_x \\ F_y \end{Bmatrix} = -\frac{1}{2}c\rho W_0 \begin{bmatrix} c_{xx} & c_{xy} \\ c_{yx} & c_{yy} \end{bmatrix} \begin{Bmatrix} \dot{u}_x \\ \dot{u}_y \end{Bmatrix} \tag{23}$$

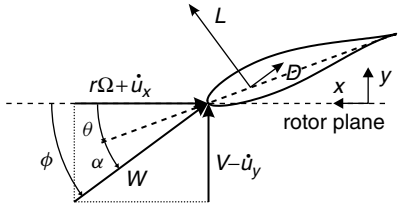

Figure 10. Velocity triangle for a blade cross-section (without induced velocities from the turbine wake)

where $W_0 = \sqrt{V^2 + r^2\Omega^2}$ is the steady relative velocity, and the diagonal elements of the damping coefficient matrix are

$$\begin{aligned} c_{xx} &= (3C_\mathrm{D} + C'_\mathrm{L} + (C_\mathrm{D} - C'_\mathrm{L})\cos 2\phi_0 - (C_\mathrm{L} + C'_\mathrm{D})\sin 2\phi_0)/2 \\ c_{yy} &= (3C_\mathrm{D} + C'_\mathrm{L} - (C_\mathrm{D} - C'_\mathrm{L})\cos 2\phi_0 + (C_\mathrm{L} + C'_\mathrm{D})\sin 2\phi_0)/2 \end{aligned} \tag{24}$$

where $()' \equiv \mathrm{d}/\mathrm{d}\alpha$, and $\phi_0 = \tan^{-1}(V/r\Omega)$ is the steady flow angle. The lift and drag coefficients and their derivatives are evaluated at the steady angle of attack $\alpha_0 = \phi_0 - \theta$.

Previous studies of quasi-steady aerodynamic damping have presented linear aerodynamic forces identical to equation (23), although their expressions for the damping coefficient have another form (see e.g. References 5, 7 and 8). These studies deal with the damping of blade vibrations, where the blade cross-sections move in straight lines in the (x, y) plane. This is the case for a blade mounted in a test stand; however, the present modal analysis of the rotating turbine shows that cross-sections move in a more elliptical motion when the blades are vibrating in a turbine mode (see Figure 7).

It is assumed that the cross-section is moving in an ellipse with the major axes parallel and perpendicular to the rotor plane, as shown in Figure 11. Using definition (20) of the effective direction of vibration θ_eff to describe the ratio of the major axes, this elliptical motion of a blade cross-section can be described by the vector

$$\mathrm{u} = a \begin{Bmatrix} \cos\theta_\mathrm{eff}\cos\omega t \\ \sin\theta_\mathrm{eff}\sin\omega t \end{Bmatrix} \tag{25}$$

where a and ω are the amplitude and frequency of the elliptical motion.

The aerodynamic damping can be approximated as the negative work done by the aerodynamic forces on the blade cross-section over one period of oscillation, $T \equiv 2\pi/\omega$. Positive aerodynamic work corresponds to negative aerodynamic damping. For the elliptical motion (25) the aerodynamic work can be derived as

$$W_\mathrm{aero} = \int_0^T \mathrm{F}^\mathrm{T}\dot{\mathrm{u}}\mathrm{d}t = -\frac{\pi}{2}\omega a^2 c\rho W_0 c_\mathrm{eff} \tag{26}$$

where c_eff is an *effective aerodynamic damping coefficient* given by

$$c_\mathrm{eff} = \frac{1}{2}(c_{xx} + c_{yy}) + \frac{1}{2}(c_{xx} - c_{yy})\cos 2\theta_\mathrm{eff} \tag{27}$$

When this coefficient is negative, the aerodynamic damping of the elliptical motion is negative. Note that the elliptical motion (25) is clockwise; the work of the linear aerodynamic forces is identical to (26) for counter-clockwise motion (this is not the case when unsteady aerodynamic effects are included).

Expression (26) shows that $c_\mathrm{eff} = c_{xx}$ for purely in-plane motion of the cross-section ($\theta_\mathrm{eff} = 0°$), whereas $c_\mathrm{eff} = c_{yy}$ for purely out-of-plane motion of the cross-section ($\theta_\mathrm{eff} = 90°$). For elliptical motion between purely in- and out-of-plane motion the effective damping coefficient lies between c_{xx} and c_{yy}. Figure 12 shows these two damping coefficients for the cross-section at 90% radius as a function of operational wind speeds of the experimental turbine analysed in this article. The grey area shows the effective damping of elliptical motion

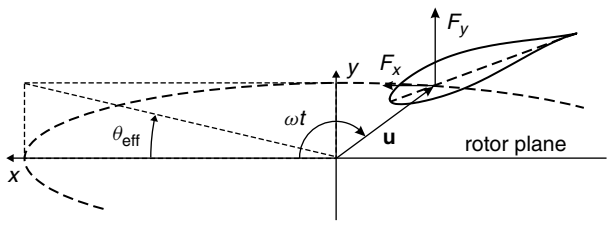

Figure 11. Elliptic motion of the blade cross-section described by the vector u (equation (25)). The effective direction of blade vibration is given by θ_eff

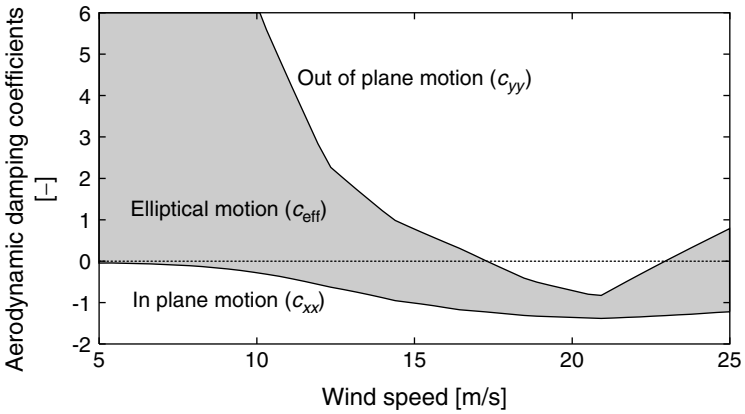

Figure 12. Quasi-steady aerodynamic damping coefficients (equation (24)) for in-plane and out-of-plane vibrations of the blade cross-section at 90% radius for the experimental 600 kW turbine.[1] *Effective damping coefficients for elliptical motion lie in the grey area between the curves*

of the cross-section. Note that $c_{xx} < c_{yy}$ at all operational wind speeds, which shows that the aerodynamic damping at this radius is always lowest for the blade vibration closest to the rotor plane.

The simple expression (26) enables a qualitative understanding of the critical parameters for stall-induced vibrations. The mean $(c_{xx} + c_{yy})/2$ determines a mean aerodynamic damping of arbitrary blade vibrations. The variation $(c_{xx} - c_{yy})/2$ about this mean determines how the damping varies with the effective direction of vibration in and out of the rotor plane. Using equation (24), the sum and difference of the two aerodynamic coefficients become

$$\begin{aligned} c_{xx} + c_{yy} &= 3C_{\mathrm{D}} + C'_{\mathrm{L}} \\ c_{xx} - c_{yy} &= (C_{\mathrm{D}} - C'_{\mathrm{L}}) \cos 2\phi_0 - (C_{\mathrm{L}} + C'_{\mathrm{D}}) \sin 2\phi_0 \end{aligned} \tag{28}$$

which shows that the drag, and the lift gradient add to the mean aerodynamic damping, e.g. a negative lift gradient decreases the mean damping. It also shows that the variation of damping with the direction of vibration depends on all aerodynamic profile coefficients weighted with the steady relative flow angle ϕ_0. It can be deduced from (28) that the aerodynamic damping of in-plane motion increases proportionally to drag but decreases proportionally to lift, lift gradient and drag gradient, because $0^\circ \leq \phi_0 \leq 90^\circ$ for most operation conditions.

References

1. Thomsen K, Petersen JT, Nim E, Øye S, Petersen B. A method for determination of damping for edgewise blade vibrations. *Journal of Wind Energy* 2001; **3**: 233–246.
2. Hansen MH, Thomsen K, Petersen JT. Rotor whirling modes and the relation to their aerodynamic damping. *2001 European Wind Energy Conference*, Copenhagen, 2001; 422–425.
3. Rasmussen F, Petersen JT, Winkelaar D, Rawlinson-Smith R. Response of stall regulated wind turbines—stall induced vibrations. *Technical Report Risø-R-691(EN)*, Risø National Laboratory, Roskilde, 1993.
4. Stiesdal H. Extreme wind loads on stall regulated wind turbines. In *Proceedings of the 16th British Wind Energy Association Conference*, Elliot G (ed.). Mechanical Engineering Publications Limited: London; 1994, 101–106.
5. Björck A, Dahlberg J, Östman A, Ganander H. Computations of aerodynamic damping for blade vibrations in stall. *1997 European Wind Energy Conference*, Dublin, 1997; 503–507.
6. Petersen JT, Thomsen K, Madsen HAa. Local blade whirl and global rotor whirl interaction. *Technical Report Risø-R-1067(EN)*, Risø National Laboratory, Roskilde, 1998.
7. Petersen JT, Madsen HAa, Björck A, Enevoldsen P, Øye S, Ganander H, Winkelaar D. Prediction of dynamic loads and induced vibrations in stall. *Technical Report Risø-R-1045(EN)*, Risø, Roskilde, 1998.
8. Rasmussen F, Petersen JT, Madsen HAa. Dynamic stall and aerodynamic damping. *ASME Journal of Solar Energy Engineering* 1999; **121**: 150–155.

9. Petersen JT, Thomsen K, Madsen HAa. Stall strips can control edgewise vibrations. *Technical Report AED–RB–6 (EN)*, Risø National Laboratory, Roskilde, 1998.
10. Anderson C, Heerkes H, Yemm R. The use of blade-mounted dampers to eliminate edgewise stall vibration. *1999 European Wind Energy Conference*, Nice, 1999; 207–211.
11. Petersen JT. The aeroelastic code HAWC—model and comparisons. In *State of the Art of Aeroelastic Codes for Wind Turbine Calculations*, vol. Annex XI, Pedersen BM (ed). International Energy Agency/Technical University of Denmark: Lyngby, 1996; 129–135.
12. Johnson W. *Helicopter Theory*. Princeton University Press: Princeton, NJ, 1980.
13. Peters DA. Fast Floquet theory and trim for multi-bladed rotorcraft. *Journal of the American Helicopter Society* 1994; **39**(4): 82–89.
14. Ziegler H. *Principles of Structural Stability* (2nd edn). Basel and Stuttgart, Birkhäuser, 1977.
15. Hansen MH. Vibrations of a three-bladed wind turbine due to classical flutter. *2002 ASME Wind Energy Symposium*, Reno, NV, 2002.
16. Leishman JG. *Principles of Helicopter Aerodynamics*. Cambridge University Press: Cambridge, 2000.

